Local Melting of Glass Material and Its Application to Direct Fusion Welding by Ps-laser Pulses

Isamu MIYAMOTO*, Alexander HORN **, Jens GOTTMANN**

*Osaka University, 2-1 Yamada-Oka, Suita, Osaka 565-0871, Japan
E-mail: isamu.miyamoto@ares.eonet.ne.jp
** Lehrstuhl fur Lasertechnik, RWTH-Aachen, Steimbachstrasse 15, 52074 Aachen, Germany

Fusion welding of glass by picosecond laser pulses is reported where laser energy absorbed by nonlinear absorption is utilized as a heat source for local internal glass melting. Laser pulses with *10ps* duration with repetition rates up to *500kHz* were focused within borosilicate glass, Schott D263, by an objective lense of NA *0.7*. The nonlinear absorptivity of the laser pulses was determined at different pulse energies, repetition rates, traveling velocities and depth of the focus position. The transient and time-averaged temperature distribution in fusion welding of glass was calculated using a thermal conduction model where heat is instantaneously deposited at different repetition rates in the rectangular solid moving linearly at a constant velocity. The experimental dimensions of the melt features agreed well with the calculated values in a velocity range of *1~100mm/s*. Excellent seam welding of two glass plates is demonstrated without cracking and thermal distortion. *10ps* laser pulses provided higher melting and joining efficiencies than sub-*ps* pulses due to the higher nonlinear absorptivity by the larger contribution of the avalanche ionization, and also provided the highest efficiencies in the existing fusion welding techniques.

DOI: 10.2961/jlmn.2007.01.0002

Keywords: picosecond laser pulse, nonlinear absorption, borosilicate glass, thermal conduction, welding, melting, glass

1. Introduction

Glass has a lot of potential applications in optics, MEMS, electrical, and biomedical field due to its excellent optical, mechanical, chemical and electrical properties. The disadvantage is, however, that only poor joining techniques are available, and thus the glass joining has to rely on the techniques using adhesive agent or interlayer, which causes poor mechanical, thermal and chemical durability.

Fusion welding is considered to be one of the most promising techniques for joining glass, since joining is accomplished without any intermediate layer and mechanical contact. It has not been accepted, however, in production because it relies on the linear absorption process where large size is melted so that cracks propagate in the molten region due to the thermal stress except for glass with low thermal expansion coefficient like fused silica **[1]**. In addition, whole thickness of the glass plates has to be melted. It is desirable to melt selectively only the internal interface of glass with overcoming the crack problems using no intermediate layers.

Ultrashort laser pulses can be used for a variety of internal processing of transparent materials, which include refractive index change, local melting and so on based on the nonlinear processes. For transparent materials, modified regions with micrometer size can be produce in the bulk of the transparent materials by the nonlinear absorption of high-intensity pulses for energy deposition **[2]**. Three-dimensional binary data storage **[3]** and direct writing of optical waveguides **[4]** were also demonstrated with *fs* lasers. In recent years, ultrashort pulse lasers with high repetition rates have been used for internal modification of transparent materials, and the effects of the heat accumulation have been discussed through the thermal conduction models **[5,6]**. These models are based on the stationary heat source with spherical or spherical Gaussian distribution, and are too simple to estimate the temperature distributions in the waveguide writing or fusion welding, since the laser energy is actually absorbed in the moving samples in the region elongated along the optical axis.

Welding of fused silica was recently reported using sub-*ps* laser pulses **[7]**, of which welding speed was limited to a very slow velocity of approximately *5μm/s* due to low repetition rate of the laser used. Advanced micro fusion welding techniques using sub-*ps* laser pulses with higher repetition rates have been developed to realize fusion welding of glass at much higher speeds **[8,9]**.

In this paper, local melting process of glass by picosecond laser pulses and its application to micro fusion welding are reported. A new thermal conduction model is developed, which is applicable not only to the fusion welding process but to the waveguide writing. The model is applied to estimate the transient temperature distribution in the laser-irradiated region and the dimensions of the resultant melted region. Based on the comparison between picosecond and femtosecond regimes, the picosecond regime is shown to be more attractive due to not only the simplicity of the laser system but the higher melting and joining efficiencies as a heat source for fusion welding of glass, because the picosecond regime provides higher nonlinear absorptivity due to larger contribution of avalanche ionization.

2. Experimental procedures

In this study, a commercially available ultrashort pulse laser system of *10ps* duration with variable repetition rates up to *500kHz* (Rapid from Lumera Laser) **[10]** was mainly used with an objective lens of NA*0.7*. An ultrashort pulse laser with *16ps* duration with a repetition rate of *1kHz* was also used for preliminary experiment with an objective lens of NA*0.9* (water immersion).

Borosilicate glass, Schott D263, with thicknesses of *1mm* and *0.2 mm* was used as the specimen. **Table 1** shows the thermal properties of Schott D263.

Table 1 Thermal properties of Schott D263 [11]

Properties	Values
Density ρ (g/cm^3)	*2.51*
Specific heat c (J/gK)[1)]	*0.82*
Thermal conductivity K ($J/s.cm.K$)[2)]	*0.0096*
Thermal diffusivity $\alpha=K/c\rho$ (cm^2/s)	*0.0046*
Melting temperature θ_m (℃)[3)]	*1051*

[1)]mean value 20~100℃, [2)] Corning 0211, [3)]forming temperature

The nonlinear absorptivity was determined by measuring the average laser powers passing through the lens and the glass specimen with a power meter. Neglecting the scattering and the reflection of the laser energy by laser-induced plasma, the nonlinear absorptivity A is given by

$$A = 1 - \frac{W_t}{W_0}\frac{1}{(1-R)^2} \quad (1)$$

where W_0 is the incident laser power to the work piece, and W_t the laser power transmitted through the specimen. The validity of this assumption is discussed later. Laser-irradiated specimens were examined by differential interference contrast (DIC), scanning electron microscopy (SEM) and white light interference (WLI) microscope.

3. Results and discussions

3.1 Preliminary study for fusion welding of glass

Laser pulses of *16ps* duration were focused by a lens of NA*0.9* into the bulk of fused silica at a repetition rate of *1kHz* with *4μJ* per pulse (*1kHz-4μJ*). A traveling velocity of the specimen of *10mm/s* resulted in single-shot modification. Each pulse provided a teardrop-shaped modified structure with a diameter *3 μm* and a length of *13μm* without cracking as shown in **Fig.1**. The teardrop structure is similar to the cone structure observed by Schaffer *et al.* using the single-pulse irradiation of *110fs* duration **[12]**. The tip of the teardrop is produced when the leading edge of the laser pulse reaches the intensity threshold for breakdown ahead of the laser focus, and then the modified region moves upwards along the optical axis following the subsequent time slices of the pulse above the threshold intensity for breakdown. The modified structure is considered to reflect the approximate intensity distribution of the laser energy deposition along the optical axis under the influence of the thermal conduction.

Assuming that *50%* of the pulse energy is nonlinearly deposited into the modified region, and thermal properties are independent of temperature, *c=0.77J/gK* and $\rho=2.2g/cm^3$, the averaged temperature rise in the teardrop region is estimated to be approximately *16,000*℃, which is much higher than the melting temperature of the glass.

The laser beam was focused to the bottom surface of the glass plates. **Figure 2** shows SEM photograph of the bottom surface where hemispheres of the molten glass with approximately 3.5*μm* in diameter are clearly visualized, which ejected out of the high temperature region of laser-irradiated region. The height of the molten hemispheres measured by WLI was approximately *300nm*, indicating that a clearance as large as several hundreds nanometers between the glass plates is allowed. This is a big advantage of the fusion welding over the solid-state bonding process, which requires intimate contact and extremely fine surface finishing. Overlapped melting was made at reduced traveling velocity without cracks as shown in **Fig. 2(b)**.

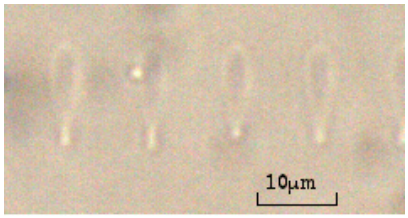

Fig.1 Internal modification of fused silica by *16ps-1kHz* pulses at *5μJ* at traveling velocity of *10mm/s*.

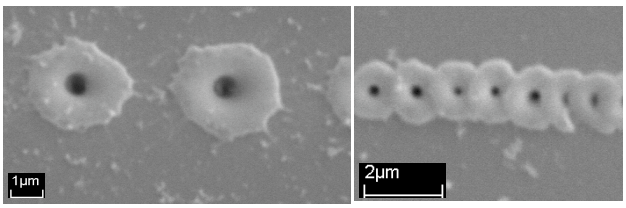

Fig.2 SEM photographs showing surface melting of Schott D263 with*16ps* pulses at *1kHz* at (a) *5μJ-5mm/s* and (b) *4μJ-0.5mm/s*.

Large stress field is produced due to extremely large temperature gradient developed by the ultrashort laser pulses, nevertheless no cracks are developed in local melting or waveguide writing in the glass. One of the possible explanations for this is small size of local melting; the stress intensity factor is proportional to the square root of the defect size, thus the stress intensity factor is reduced due to very small molten size caused by ultrashort laser pulses. It is required to do further work to properly explain.

3.2 Thermal conduction model

A thermal conduction model for fusion welding of glass by ultrashort laser pulses was developed where instantaneous heat source is generated periodically into a rectangular region moving in an infinite solid. This model can be also applied to calculate the waveguide writing.

The thermal conduction equation

$$\frac{\partial^2\theta}{\partial x^2} + \frac{\partial^2\theta}{\partial y^2} + \frac{\partial^2\theta}{\partial z^2} = \frac{1}{\alpha}\frac{\partial\theta}{\partial t}$$

is satisfied by the following solution **[13]**

$$\theta(x,y,z;t) = \frac{Q}{8\{\pi\alpha(t-t')\}^{2/3}}\exp\left\{-\frac{(x-x')^2+(y-y')^2+(z-z')^2}{4\alpha t}\right\}, \quad (2)$$

where α is thermal diffusivity, Q pulse energy and t time. Using this solution, the temperature rise $\theta(x,y,z;t)$ due to an arbitrary heat source is given by:

$$\theta(x,y,z;t)=\frac{1}{8(\pi\alpha)^{2/3}}\int_0^{\infty}dt'\int_{-\infty}^{\infty}\int_{-\infty}^{\infty}\int_{-\infty}^{\infty}\frac{Q(x',y',z';t-t')}{(t-t')^{3/2}}\cdot\exp\left\{-\frac{(x-x')^2+(y-y')^2+(z-z')^2}{4\alpha(t-t')}\right\}dx'dy'dz'. \quad (3)$$

We assume that instantaneous laser energy Q is periodically incident at a repetition rat of f to the rectangular solid uniformly, which starts from $x=-\infty$ and moves at a constant velocity v along the x-axis in an infinite solid. The assumption of the 'instantaneous' heat source is valid, since the heat diffusion during the pulse duration of *10ps* is negligible. Assuming that the latest pulse is deposited at $t=0$ at which the center of the moving rectangular solid locates at the origin of the coordinate (**Fig. 3**), the temperature rise at (x,y,z) at time t, $\theta(x,y,z;t)$, in a quasi-steady state is given by $(T=1/f)$.

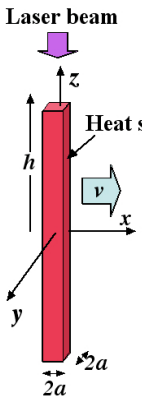

Fig.3 Rectangular solid heat source moving at a constant velocity v along the x-axis.

$$\theta(x,y,z;t)=\frac{AQ}{64c\rho r}\sum_{i=0}^{\infty}\left(erfc\frac{\xi+i\upsilon\Xi^2/2-\delta}{\tau\sqrt{(i\Xi^2/\tau^2+1)}}-erfc\frac{\xi+i\upsilon\Xi^2/2+\delta}{\tau\sqrt{(i\Xi^2/\tau^2+1)}}\right)\cdot\left(erfc\frac{\psi-\delta}{\tau\sqrt{(i\Xi^2/\tau^2+1)}}-erfc\frac{\psi+\delta}{\tau\sqrt{(i\Xi^2/\tau^2+1)}}\right)\cdot\left(erfc\frac{\zeta-\eta}{\tau\sqrt{(i\Xi^2/\tau^2+1)}}-erfc\frac{\zeta+\eta}{\tau\sqrt{(i\Xi^2/\tau^2+1)}}\right), \quad (4)$$

$$where\quad erfcU=\frac{2}{\sqrt{\pi}}\int_U^{\infty}\exp(-u^2)du.$$

Here A is absorptivity of the laser pulse, $2a$ focus diameter of the laser beam, $2h$ length of heat source along the z-axis, c the specific heat and ρ density. In this equation, the following non-dimensional parameters are introduced.

$$r^3=a^2h,\ \xi=\frac{x}{r},\ \psi=\frac{y}{r},\ \varsigma=\frac{z}{r};\ \delta=\frac{a}{r}=n^{-1/3},\quad \eta=\frac{h}{r}=n^{2/3},\ \tau=\frac{1}{r}\sqrt{4\alpha t},\ \Xi=\frac{1}{r}\sqrt{4\alpha T},\ \upsilon=\frac{vr}{2\alpha}. \quad (5)$$

The temperature distributions in a quasi-steady state was calculated at different pulse repetition rates at an averaged power of $Qf=0.2W$, assuming that the rectangular solid heat source is of $a=1\mu m$ and $h=10\mu m$. **Figure 4** shows the temperature distributions at *100mm/s* along the x-axis ($y=z=0$) at repetition rates of *100kHz*, *500kHz* and *1MHz* at different time after the latest laser pulse arrival. The temperature in the laser-irradiated region at the moment of the pulse irradiation ($t=0$, light blue line) increases with decreasing f due to the increased pulse energy. Then the temperature in the laser-irradiated region is decreased due to the thermal diffusion down to the lowest temperature at time $t=0.999T$ (green line), corresponding to the time just before the next pulse arrival. The temperature at $t=0.999T$ decreases as the pulse repetition rate f decreases due to increased cooling time.

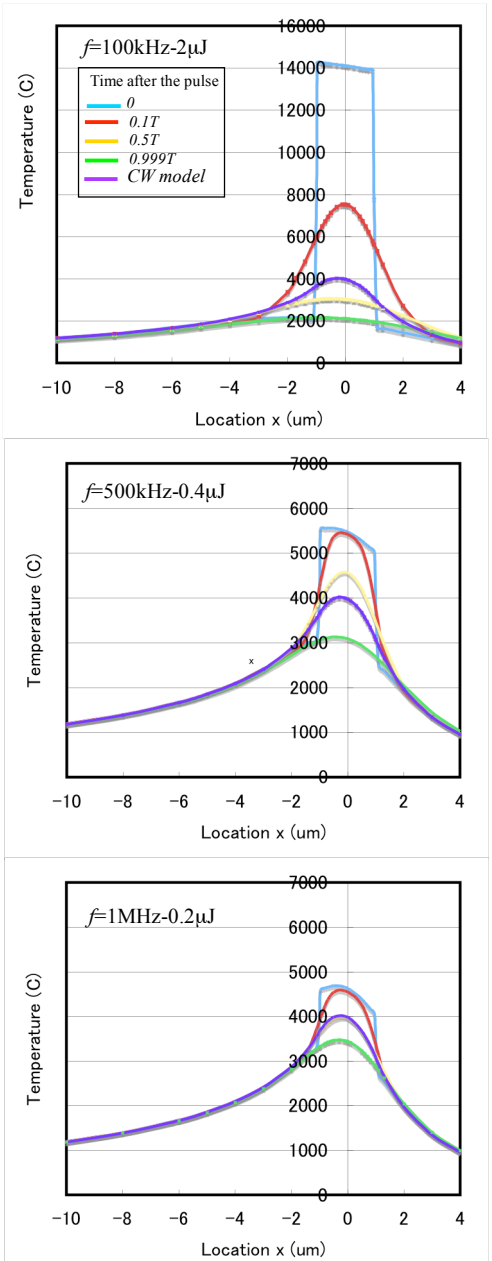

Fig.4 Temperature distribution along the x-axis ($y=z=0$) calculated with pulse and CW models. ($W=0.2W$, $a=1\mu m$, $h=10\mu m$, $v=100mm/s$).

A thermal conduction model due to a CW (continuous wave) heat source was also developed. Assuming that the CW laser with an average power $W=fQ$ is incident to the rectangular region uniformly, the temperature rise in a steady state is written in a simpler form given by

$$\Theta(\xi,\psi,\zeta)=\int_0^{\infty}\left\{erfc\left(\frac{\xi-\delta}{\tau}+\frac{\upsilon\tau}{2}\right)-erfc\left(\frac{\xi+\delta}{\tau}+\frac{\upsilon\tau}{2}\right)\right\}\cdot\left(erfc\frac{\psi-\delta}{\tau}-erfc\frac{\psi+\delta}{\tau}\right)\left(erfc\frac{\zeta-\delta}{\tau}-erfc\frac{\zeta+\delta}{\tau}\right)\tau\cdot d\tau \quad (6)$$

$$where\quad \theta(x,y,z)=\frac{AQf}{128Kr}\Theta(\xi,\psi,\zeta).$$

Examples of the temperature distributions due to the CW mode are also plotted in **Figs. 4** with dark blue lines. **Figure 5** shows the lateral distribution of the maximum temperature attained in a thermal cycle along the *x*-axis in the pulse and CW modes. The maximum cycle temperatures due to pulse mode near the heat source region are higher than those of CW mode, and increase with decreasing the repetition rate. They agree, however, well with values of the CW mode in a region *~3μm* apart from the laser axis, indicating the temperatures of the pulse mode can be approximated by the CW model outside of this region. So **Eq(6)** can be used to estimate the size of melt dimensions whereas **Eq(4)** has to be used to calculate the temperature rise within the laser-irradiated region for discussing the laser-matter interaction as is described in **3.3**.

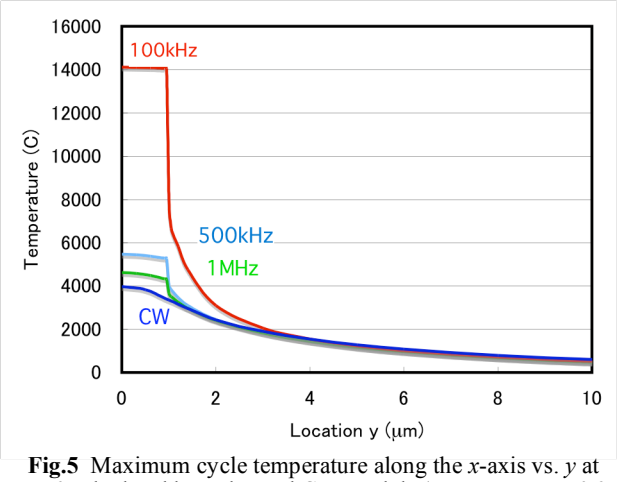

Fig.5 Maximum cycle temperature along the *x*-axis vs. *y* at *z=0* calculated by pulse and CW models (average power *0.2W*, *a=1μm*, *h=10μm*, *v=100mm/s*).

3.3 Nonlinear absorptivity of ps lser pulses

In fusion welding of glass, the energy of the ultrashort laser pulse is transferred from the laser-excited electrons to the lattice after the laser pulse is gone unlike the case of *ns* laser pulses. The efficiency of the fusion welding directly depends on the nonlinear absorptivity of the ultrashort laser pulses. There are two mechanisms responsible for the nonlinear absorption of ultrashort laser pulses, photoionization and avalanche ionization.

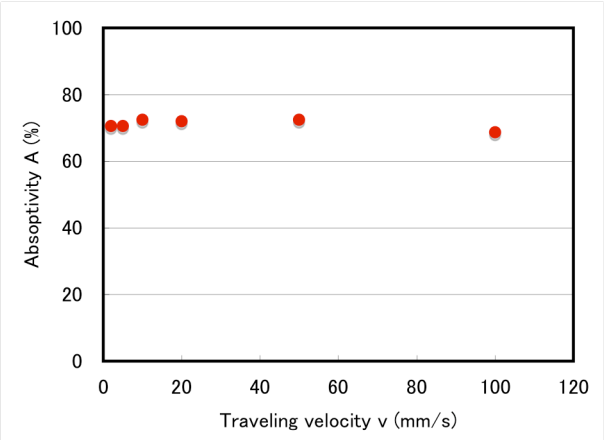

Fig.6 Nonlinear absprptivity vs. traveling velocity of the specimen at *10ps-3μJ* at *100kHz*.

The nonlinear absorptivity of Schott D263 at *10ps* duration was determined from **Eq(1)** at different pulse energies, repetition rates, traveling velocities and focus positions. High reflectivity of the laser-induced surface plasma has been reported with *fs* laser pulses **[14,15]**. In contrast to the surface plasma, the laser reflection by the plasma induced in the bulk can be neglected on the basis of the laser-plasma interaction model described below.

The cone- or the teardrop-shaped structures seen in **Fig. 1** are considered to be the result of different temporal slices of an above-threshold pulse producing breakdown at different positions in the bulk **[16]**; the breakdown starts at the leading edge of the converging laser pulse when the laser intensity exceeds the breakdown threshold near the focus to form the tip of the cone or teardrop. Subsequent time slices of the laser pulse have enough energy to produce breakdown upstream or the focus where beam diameter is larger. Breakdown proceeds upwards, leading to the cone- or the teardrop-shaped structure, reflecting the shape of the focusing laser beam. Then it is expected a steep density distribution is produced in the laser-plasma interaction region, where the electron density is highest at the interaction front and decreases along upward direction. When the electron density is less than the critical density at the interaction front, a part of the incident laser energy transmits through the specimen. On the other hand, the laser beam reflected and scattered as well is absorbed by the high-density electron layer existing above the interaction front, when the electron density at the interaction front exceeds the critical electron density. The validity of this model is examined by comparing the experimental melt dimensions with the values calculated by the thermal conduction analysis using the absorbed laser energy determined from Eq(1) in **3.4**.

Figure 6 shows the nonlinear absorptivity plotted vs. traveling velocity at *100kHz*. Little change in the absorptivity is observed at different traveling velocities within the conditions tested, and so the nonlinear absorptivity was determined at a traveling velocity of *1mm/s* hereafter.

The nonlinear absorptivity of *10ps*-pulses is plotted vs. pulse energy in **Fig. 7**. The absorptivity data are also plotted with sub-picosecond laser pulses (*406fs* at *1MHz* and *325fs* at *100kHz*) focused by a lens of NA*0.65* **[8]**, which is nearly equal to NA*0.7* used in the present study. There are three parameters influencing the nonlinear absorptivity, pulse energy, pulse duration and pulse repetition rate as is described bellow.

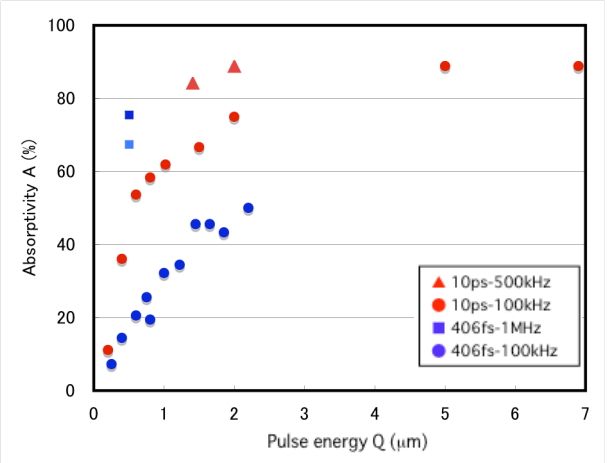

Fig.7 Absorptivity vs. pulse energy at *10ps* duration at different repetition rates. Data with sub-*ps* pulses **[8]** are also plotted for comparison.

The nonlinear absorptivity is seen to increase with increasing pulse energy for both pulse durations. This is because photoionization rate increases with increasing laser intensity **[17]**.

When compared at a condition of *0.5μJ-100kHz*, the nonlinear absorptivity of *10ps* is *2~3* times higher than that of *325fs* pulses, although the laser intensity of *10ps* is approximately *30* times lower than that of *325fs*. This is because *10ps*-pulse duration is long enough for the growth of the electron density in the conduction band by the avalanche ionization. The nonlinear absorptivity of *10ps*-pulses reaches as high as *90%* at *500kHz*, which indicates that the electron density grows until the critical plasma density, and efficiently absorbs laser energy by free-carrier absorption **[17,18]**. The absorptivity as high as *90%* also indicates that the critical electron density was reached at very beginning of the pulse duration, *1~2 ps* at most.

In the sub-*ps* laser pulses, the nonlinear absorptivity of *1MHz* is seen to be *3~4* times larger than that of *100kHz* at *0.5μJ*. This can be explained by the temperature just before the pulse arrival θ_B (t=*0.999T*), which determines the density of thermally excited electrons in conduction band. The temperature θ_B calculated at *0.5μJ* by Eq(4) was approximately *8500℃* and *1200℃* for *1MHz* and *100kHz*, respectively **[8]**. In the former case, a simple calculation estimates that approximately *0.4%* of electrons in valence band is thermally excited in the conduction band in addition to the photoionization. It is considered that these seed electrons are increased in the very beginning of the laser pulse by avalanche ionization so that the laser beam is thereafter absorbed by free-carrier absorption efectivley. In the latter case, on the other hand, very limited number of the seed electrons are promoted to the conduction band only by photoionization, results in lower absorprivity. When compared at *100kHz* between *325fs* and *10ps* pulse durations, the former provides considerably lower absorprivity because the pulse duration is too short to increase the electron by the avalanche ionization.

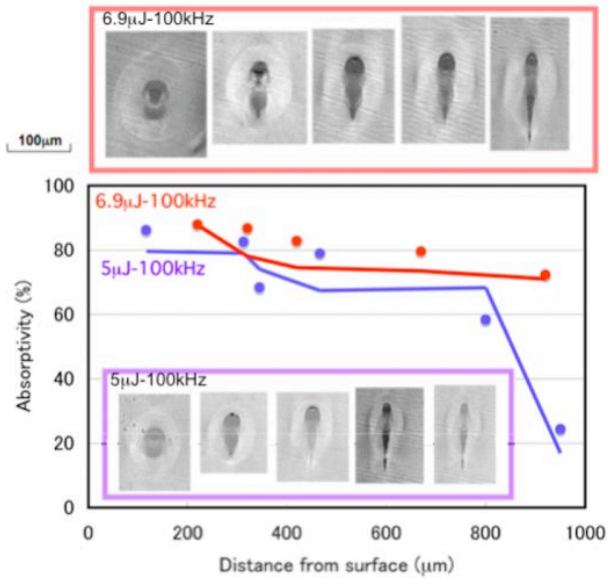

Fig.8 Absorptivity vs. focus position in glass plate of Schott D263at *5.0μJ* and *6.9μJ* at *100kHz* with*10ps* laser pulses. Solid lines indicate the absorptivity calculated from experimental melt dimensions.

Based on the above discussion, it is concluded that higher repetition rates are essential for enhancing nonlinear absorptivity in sub-*ps* pulses. In contrast, in *10ps*-pulses higher nonlinear absorptivity can be attained even at rather lower repetition rates, since much longer time is available for the growth of the electron density by the avalanche ionization. It is suggested that pulse duration of *1~10ps* is appropriate pulse duration for local melting and hopefully waveguide writing of glass because laser energy is deposited on a time scale shorter than the thermal diffusion time with accompanying higher nonlinear absorptivity.

Figure 8 shows the nonlinear absorptivity for the *10ps*-pulse duration plotted vs. focus position at *100kHz*. The-nonlinear absorptivity is approximately *90%* at the depth of *200μm*, providing the modified dimensions as large as *145μm* height and *128μm* width at *6.9μJ* in contrast to the demonstration by Eaton *et al.* **[6]** that no heat accumulation is expected at *100kHz*. The heat accumulation becomes pronounced even at a rather low repetition rate of *100kHz* at high average laser power, as is described later. In **Fig. 8**, the area of melt cross-section decreased with increasing the distance from the top surface, and the shape of the inner region of the modified zone becomes oblong as the position of the focus becomes deeper with accompanying the reduced absorptivity. Although the similar tendency was observed at both pulse energies, *6.9μJ* and *5.0μJ*, the effect of the aberration was more pronounced at lower pulse energy. Detailed mechanism is not known, but it is suggested that the effect of the aberration of the objective lens in the bulk cannot be neglected where the lens was adjusted to provide best focus at the depth of *200μm* in **Fig. 8**. In fact, the appreciable increase in the absorptivity at deeper positions was observed by changing the optimum depth to the deeper positions.

3.4 Thermal conduction analysis in fusion welding glass by picosecond laser pulses

Figure 9 shows the cross sections of the modified zone made by *10ps* laser pulses at *700mW* (*500KHz-1.4μJ*) at different traveling velocities. The modified zone consists of the teardrop-shaped inner region extended along the optical axis and the surrounding ellipse-shape like the case of sub-*ps* laser pulses **[4,8]**. The dimensions of the inner and outer regions were measured as a function of the traveling velocity of the specimen, and plotted in **Figs. 10** and **11**.

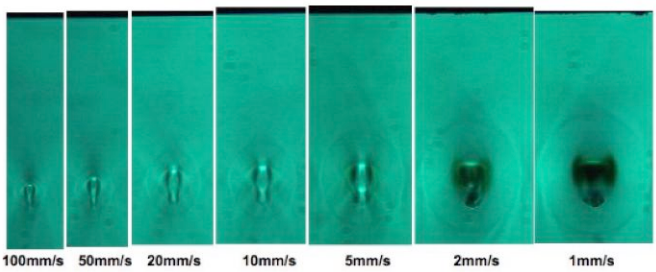

Fig.9 Crosse sections of molten zone made with *500kHz-1.4μJ* at *10ps* for Schott D263 at various traveling velocities.

In **Fig. 10**, the vertical size of the inner region is plotted vs. traveling velocity along with the sub-picosecond laser pulses at *1MHz-500μJ* for comparison **[8]**. Little differen-

ce in the vertical size of the inner area was observed between two different pulse durations.

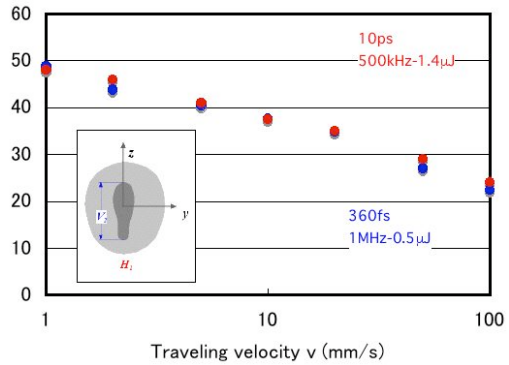

Fig.10 Vertical size of inner region (teardrop) V_2 at *10ps* (*500kHz-1.4μJ*). For calculation, $2h=0.9*V_2$ was assumed.

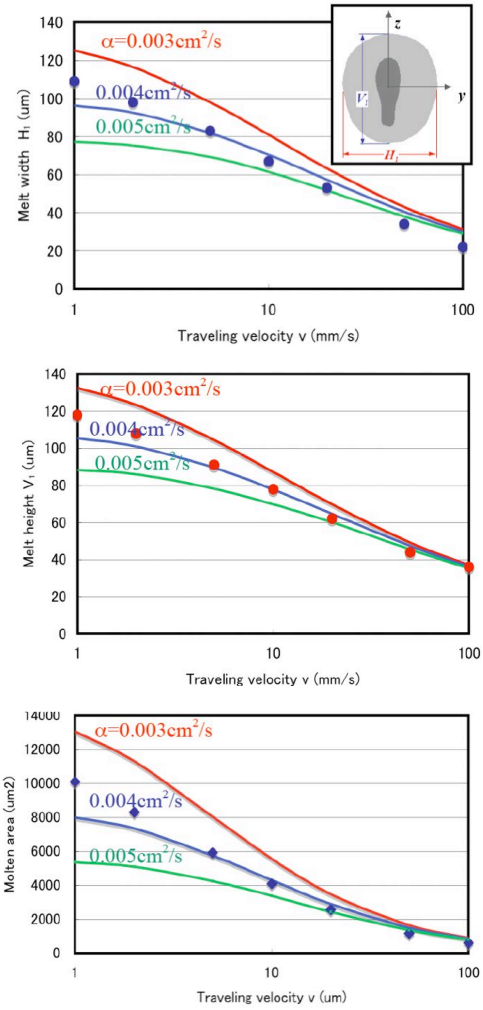

Fig.11 Calculated molten sizes (H_1 and V_1) and cross sectional area S vs. traveling velocity with *10ps* laser pulses at *700mW* (*500kHz-1.4μJ*) for different values of thermal diffusivity α using absorptivity $A=84.2\%$ and h shown in Fig. 10. Data points are experimental values.

The inner region is analogous in shape to the single shot modification shown **Fig. 1**, indicating it was produced by the direct effect of the laser pulse **[8]**. It was assumed that the laser energy absorbed by the electrons in conduction band is completely transferred to the lattice in a region of the rectangular solid with diameter of $2a$ and length $2h=\gamma\times V_2$ uniformly. The temperature distributions at *500kHz-1.4μJ* were calculated at different traveling velocities using the measured nonlinear absorptivity of $A=84.2\%$, assuming $\gamma=0.9$ arbitrarily to take into consideration that the inner zone also expanded to some extent due the thermal conduction.

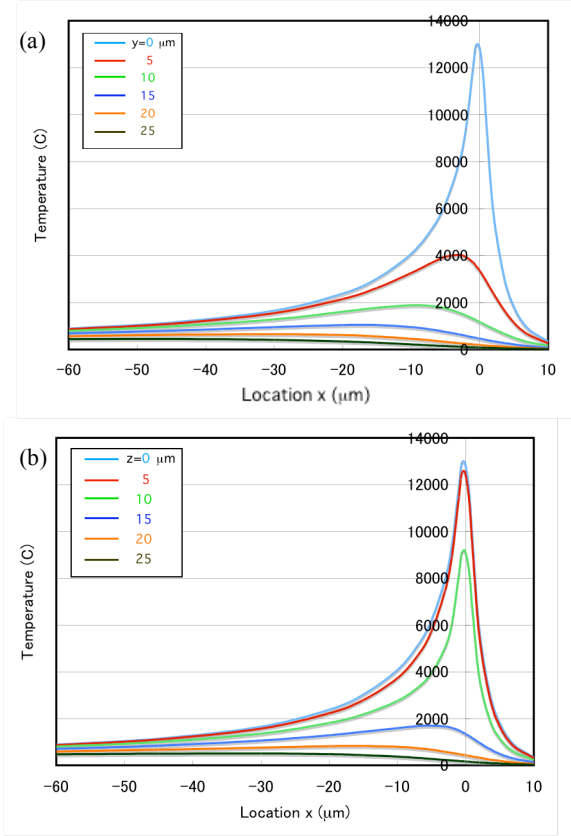

Fig.12 Temperature distributions along the x-axis in (a) xy-plane at $z=0$ and (b) xz-plane at $y=0$ calculated with *700mW, 100mm/s and* $\alpha=0.004cm^2/s$.

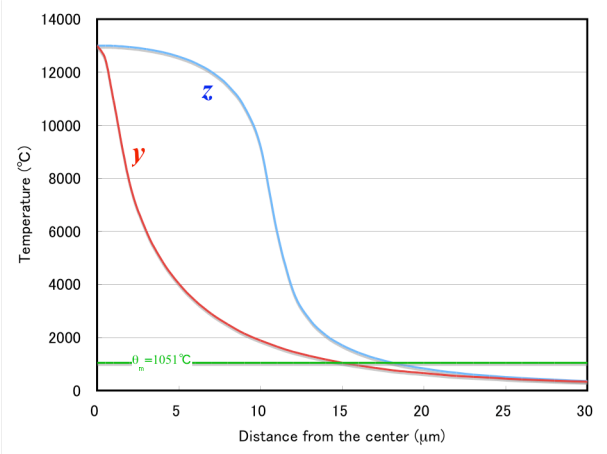

Fig.13 Maximum cycle temperature distribution along the y- and the z-axes calculated with *700mW*, *100mm/s* and $\alpha=0.004cm^2/s$.

Figure 12 shows examples of steady temperature distributions in the xy-plane ($z=0$) and the xz-plane ($y=0$) calculated with *700mW* and *100mm/s*. Each curve indicates a temperature cycle, of which maximum value is reached behind the heat source. **Figure 13** shows the distribution of the maximum cyclic temperature along the y- and the z-axes. The temperature corresponding to an isothermal line

of the inner modified region was estimated to be approximately *4,000~ 4,500℃*. The values of the melt width H_1, height V_1 and cross sectional area $S=\pi H_1 V_1/4$ determined at the temperature $\theta_m=1051℃$ are plotted in **Fig. 11**.

In the higher traveling velocity region, the calculated dimensions agree well with the experimental values with the thermal diffusivity $\alpha=0.005cm^2/s$, which is close to $\alpha=K/c\rho=0.0046cm^2/s$ corresponding to the thermal conductivity $K=0.009$ *J/s.cm.K* shown in **Table 1**. It is seen, however, that the calculated values almost saturate at traveling velocities around *5mm/s* as the traveling velocity decreases, whereas the experimental values are still increasing even at *1mm/s*, showing appreciable discrepancy between the calculated and experimental values using $\alpha=0.005cm^2/s$. Similar discrepancy was observed in the static exposure in borosilicate glass with femtosecond laser pulses of *25MHz* at pulse number larger than 10^4 **[5]**. The calculated values agree well with the experimental values by adopting smaller thermal diffusivities at lower traveling velocities. This indicates that the effective thermal diffusivity is decreased when high temperature region extends widely.

In order to examine the validity of the aforementioned assumption in **2** that the reflection and the scattering of laser energy by the plasma induced in the bulk is negligible, the absorptivity was calculated using the experimental melt dimensions. It is seen that the calculated absorptivity plotted with solid lines in **Fig. 8** agrees well with the experimental values, which range widely between approximately 20% and 90%.

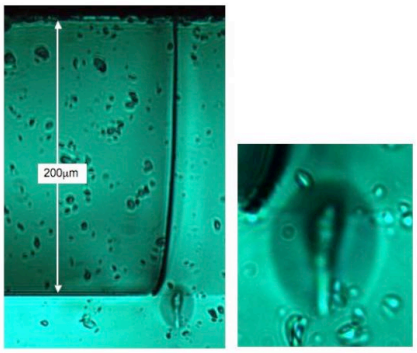

Fig.14 Examples of weld joint of D263 with thickness of *1mm* and *0.2mm* with *10ps* laser pulses at *0.6μJ-500kHz* at *10mm/s*.

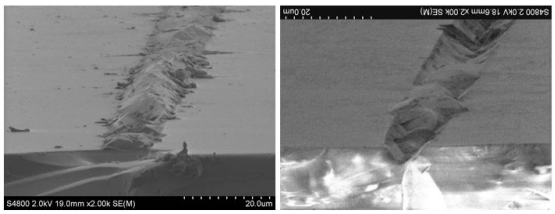

Fig.15 SEM photograph of pealed-off weld joint.

3.5 Applications to welding

Figure 14 demonstrates an example of the cross section of lap joint of two glass plates with thickness of *200μm* and *1mm*. The *10ps* laser pulses were focused aiming at the interface from the *200μm*-thick plate side. It happened that the glass plate of *200μm* in thickness was broken near the weld joint by the mechanical force applied in the polishing processes of the samples embedded in epoxy resin. Nevertheless the weld joint is not separated, indicating joining strength is favorably high. **Figure 15** shows SEM photographs of the peeled-off weld joint. The sample was broken in an irregular plane apart from the original interface by brittle fracture indicating that the two plates were strongly joined.

A melting efficiency η and a joining rate R were determined to estimate the throughput of the welding. The melting efficiency η is defined by the ratio of the power required for elevating the volume of the weld bead up to the melting temperature to the laser power, and is given by

$$\eta = \frac{Svc\rho\theta_m}{W_0} \tag{7}$$

where S is given by $\pi H_1 V_1/4$. As is seen in **Fig.16**, η increases with increasing traveling velocity reaching approximately *40%* at *100mm/s*.

The joining efficiency R is defined by the joint area of the two plates per unit laser energy, and is given by

$$R = \frac{vH_1}{W_0}. \tag{8}$$

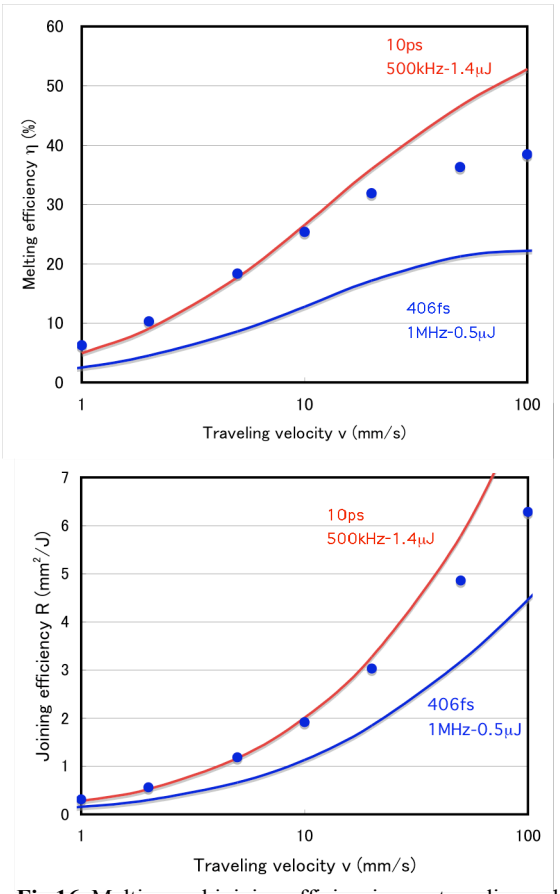

Fig.16 Melting and joining efficiencies vs. traveling velocity by 10ps laser pulses (*10ps*, *500kHz-1.4μJ*α*= 0.003cm*^{2}). Blue lines show the values obtained with sub-ps pulses **[8].**

As shown in **Fig.16**, the joining efficiency increases with increasing traveling velocity, reaching as large as approximately $6.5mm^2/J$. This value is much higher than the maximum value of $2.5mm^2$/J attained in metal welding with

single-mode fiber laser by one of the authors **[19,20]**, indicating that fusion welding of glass by *ps* laser pulses are most efficient in the existing welding technologies.

The efficiencies in glass welding by sub-*ps* laser pulses are also plotted in the figure for comparison. It is seen that the efficiencies of *ps* laser pulses are considerably higher than those of sub-*ps* laser pulses **[8]**. This is attributed to the facts that the nonlinear absorptivity of *ps* laser pulses in comparison with sub-*ps* laser pulses as discussed in **3.3**, and that higher average power can be easily obtained in *ps* regime.

4. Conclusions

Local-melting characteristics of borosilicate glass was analyzed using *10ps* laser pulses with maximum repetition rate of *500kHz* in comparison with sub-*ps* laser pulses. A new thermal conduction model was developed to calculate transient temperature distribution during laser irradiation. The model provides useful information for analysis and optimization of ultrashort pulse laser processing not only in fusion welding but in optical waveguide writing. The results obtained are summarized as follows.

(1) A novel fusion welding technique was developed using *10ps* laser pulses without cracks and thermal distortion, opening a new promising application field of ultrashort laser pulse.

(2) Nonlinear absorprivity of *10ps* laser pulses increases with increasing pulse repetition rate and pulse energy, and is higher than the value of sub-*ps* laser pulses due to larger contribution of avalanche ionization. Maximum nonlinear absorptivity as high as *90%* was attained.

(3) The thermal conduction model agreed well with the experimental melt dimensions in the range of traveling velocity between *1* and *100mm/s*. The effects of laser parameters on the nonlinear absorptivity were discussed based on the temporal temperature distributions calculated by the model.

(4) Sound fusion welding of glass plates was demonstrated where only the interface of the glass plates is locally melted. In addition to the system simplicity, *ps* regime is superior to *fs* regime in terms of higher joining efficiency due to its higher nonlinear absorptivity. Fusion welding glass by ultrshort pulse laser provides much higher joining efficiency than existing metal welding techniques.

Acknowledgments

The authors wish to thank D. Wortmann and I. Mingareev, Lehrstuhl fur Lasertechnik, RWTH-Aachen, for the informative discussions, and to F. Sari and M. Rupf, Fraunhofer Institute, ILT, for preparing the weld specimens.

References

[1] Y. Arata, H. Maruo, I. Miyamoto, S.Takeuchi: Proc. 7th International Conference on Electron and Ion Beam Science and Technology, p.111 (1976)

[2] K. M. Davis, K. Miura, N. Sugimoto, K. Hirao: Optics Letters, **21**, p.1729 (1996)

[3] E. N. Glezer, M. Milosavljevic, L. Huang, R. J. Finlay, H. Her, J. P. Callan, E. Mazur, Opt. Lett, **21**, 2023 (1996)

[4] S. Nolte, M. Will, J. Burghoff, A. Tünnermann: J. Modern Optics **10**, p.2533 (2004)

[5] C. B. Schaffer, J. F. Garcia, E. Mazur: APPL. PHYS. **A76**, p.351 (2003)

[6] S. M. Eaton, H. Zhang, P. Herman, F. Yoshino, L. Shah, J. Bovatsek, A. Y. Arai: Optics Express, **13**, p.4708 (2005)

[7] T. Tamaki, W. Watanabe, J. Nishii, K. Itho: Japanese J. Appl. Phys. **44**, p.L687 (2005)

[8] I. Miyamoto, A. Horn, D. Wortmann, J. Gottmann, F. Yoshino: Proc. LAMP2006 (2006) 052323-1

[9] J. Bovatsek, A. Arai, C. B. Schaffer: Proc. CLEO'06 (2006) to be published

[10] C. Ratermann, R. Knappe, T. Herrmann, B. Henrich, A. Nebel: Proc. ICALEO2005 p.119 (2005)

[11] Private communication with Dr. Hermanns, Schott Glass

[12] C. B. Schaffer, A. O. Jamison, E. Mazur: Appl. Phys. Lett., **84**, p. 1441 (2004)

[13] H. S. Carslaw, J. C. Jeager: Conduction of heat in solid, Oxford at the Clarendon Press (1959)

[14] D. von der Linde, H. Schuler: J. Opt. Soc. Am. B, 13, p.216 (1996)

[15] T. Q. Jia, H. X. Chen, M. Huang, F. L. Zhao, X. X. Li, S. Z. Xu, H. Y. Sun, D. H. Feng, C. B. Li, X. F. Wang, R. X. Li, Z. Z. Xu, X. K. He, H. Kuroda: Phys. Rev. B 73 054105 (2005)

[16] C. B. Schaffer, A. O. Jamison, E. Mazur: Appl. Phys. Lett, 34, p.1441 (2004)

[17] B. C. Stuart, M. D. Feit, S. Herman, A. M. Rubenchik, B. W. Shore, M. D. Perry: Phys. Rev. B**53**, p. 1749 (1996)

[18] M. Lenzner, J. Küger, S. Sartania, Z. Cheng, Ch. Spielmann, G. Mourou, W. Kautek, F. Krausz: Phys. Rev. Lett. **80**, p.4076 (1998)

[19] G. Deadon: Proc. 3rd International WLT-Conference on Laser in Manufacturing, p.615 (2005)

[20] I. Miyamoto, S-J. Park, T. Ooie: Proc. ICALEO'02 , ISBN 0-912035-72-7 (2002)

(Received: July 11, 2006, Accepted: January 9, 2006)